Macro- and microstructures in ordinary chondrites: Implications for impact deformation and annealing processes

A. Ruzicka[1], J.M. Friedrich[2], R. Hugo[1], and M. Hutson[1]. [1]Cascadia Meteorite Laboratory, Department of Geology, Portland State University, 17 Cramer Hall, 1721 SW Broadway, Portland OR 97207, USA. [2]Department of Chemistry, Fordham University, Bronx NY 10458 and Department of Earth and Planetary Sciences, American Museum of Natural History

INTRODUCTION

Impact deformation of chondrites results in metal grain shape foliation and a decrease in porosity [1-5]. We re-examine evidence for these processes in light of additional data for ordinary chondrites, including micro-computerized tomography (µCT) data for metal grain fabric in three dimensions, olivine shock stages [16] by optical microscopy (OM), and olivine microstructures by transmission electron microscopy (TEM). Some samples were measured for porosity using bead methods and He pycnometry.

Ordinary chondrites of various groups (H, L, LL) were studied. Meteorites included both "reference" or baseline L6 chondrites of different shock stages, and H6 and LL6 chondrites identified previously as either post-shock-annealed or hot-deformed.

Samples: Reference & annealed

Reference or baseline meteorites: L6 chondrites, no distinctive annealing history

Annealed meteorites: H6 and LL6 chondrites that show evidence for distinctive thermal history, either post-shock-annealed or hot-deformed [5-15]

Table 1.

Samples and OM data

Meteorite	Type	Rationale	Conventional &[weighted] shock stage	Comment
Park	L6	baseline	S1 [S1.35]	
GRO 85209	L6	baseline	S1	conventional shock stage confirmed
Holbrook	L6	baseline	S3 [S2.38]	breccia—S1 thru S4-dominant
Bruderheim	L6	baseline	S4 [S3.78]	
Leedey	L6	baseline	S4 [S3.94]	
Alfianello	L6	baseline	S5 [S4.17]	
Tenham	L6	baseline	S5 [S4.26]	
Morrow County	L6	baseline	S5 [S4.46]	
Kernouve	H6	annealed	S1 [S1.13]	metal veins; evidence for subgrains
Portales Valley	H6/7	annealed	S1 [S1.16]	metal veins; evidence for subgrains
MIL 99301	LL6	annealed	S1 [S1.60]	S1-dominant, but contains admixture of more highly shocked material; evidence for subgrains
Butsura	H6	annealed	S1 [S1.63]	metal veins; breccia—S1-dominant, but contains admixture of more highly shocked material
Spade	H6	annealed	S4 [S2.39]	breccia—S1 & S4-dominant; evidence for subgrains
Saint-Severin	LL6	annealed	S4 [S3.25]	breccia—S2- thru S4-dominant
Estacado	H6	other	S1 [S1.26]	evidence for subgrains
Queen's Mercy	H6	other	S2	literature data only for shock

Optical microscopy

- Olivine grains assigned to optical shock stages [16]
- Conventional shock stage given by highest shock stage shown by at least 25% of grains [16] (Table 1)
- Weighted shock stage equated to mean of grain shock stages (Table 1)
- Some meteorites have relatively non-uniform grain shock stages (e.g. Holbrook, Saint-Séverin, Spade, Butsura, MIL 99301)—interpreted as evidence for brecciation (Table 1)
- Evidence for subgrain boundaries found in olivine from some meteorites (Portales Valley, MIL 99301, Kernouvé, Spade, Estacado, possibly Park and Saint-Séverin (Fig. 1)—interpreted as evidence for post-deformation annealing

Fig. 1. Cross-polarized transmitted light micrographs of an olivine grain (green, at center) from Portales Valley in two different stage positions, showing a low-angle grain boundary between regions 1 and 2 which have different crystal orientations. The low angle boundary is interpreted as a subgrain boundary. Fringes (b) indicate a dipping contact at the boundary.

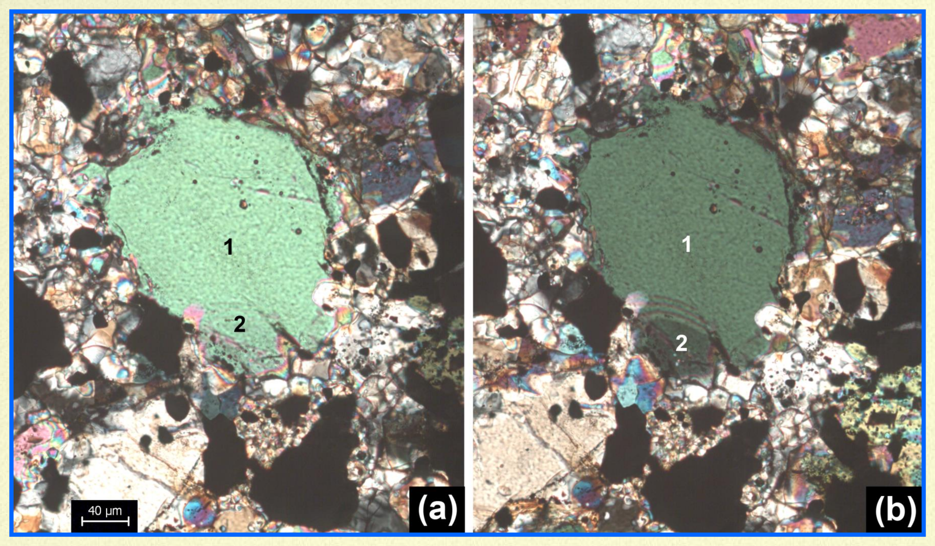

Metal grain shape orientation

- Measure preferred orientation of metal by using long axis of ellipsoids fit to metal grains
- Metal shows variable amount of preferred orientation in different meteorites (e.g., Park low degree, Tenham high degree) (Fig. 2)
- Quantify preferred orientation by strength factor C (higher C, more preferred orientation)
- Preferred orientations represent foliations

Fig. 2 Stereoplots showing distribution of metal grain long axes in Park and Tenham. Colors represent relative orientation densities (red-higher, blue-lower). Note the different color scales for Park and Tenham. In Park, there is little preferred orientation, whereas in Tenham, there is a strong preferred orientation. Preferred orientations of metal in chondrites such as Tenham represent foliations.

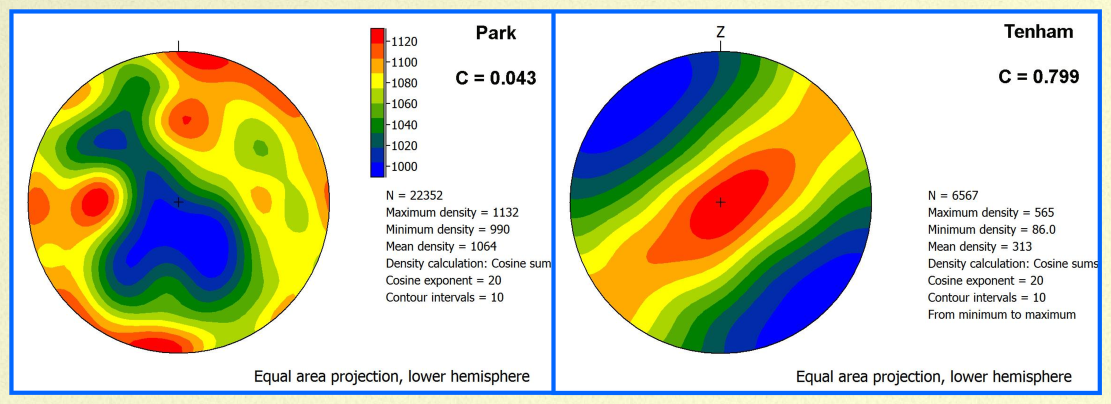

Transmission electron micros.

- TEM used to characterize dislocation density and other microstructures in olivine
- Park, Bruderheim, Leedey, Morrow County, Kernouvé, Portales Valley, and MIL 99301 studied
- Find overall correlation between dislocation density (geometric average) and weighted shock stage for reference L chondrites, but annealed chondrites Kernouvé, Portales Valley and MIL 99301 have much lower overall dislocation density
- Subgrain boundaries are prominent in the annealed chondrites (Fig. 3), rare in the reference L chondrites
- Data can be explained by microstructural recovery, caused by prolonged annealing following deformation in Kernouvé, Portales Valley, and MIL 99301

Fig. 3. TEM weak beam dark field image of olivine in Kernouvé showing a relatively low dislocation density and the presence of subgrain boundaries.

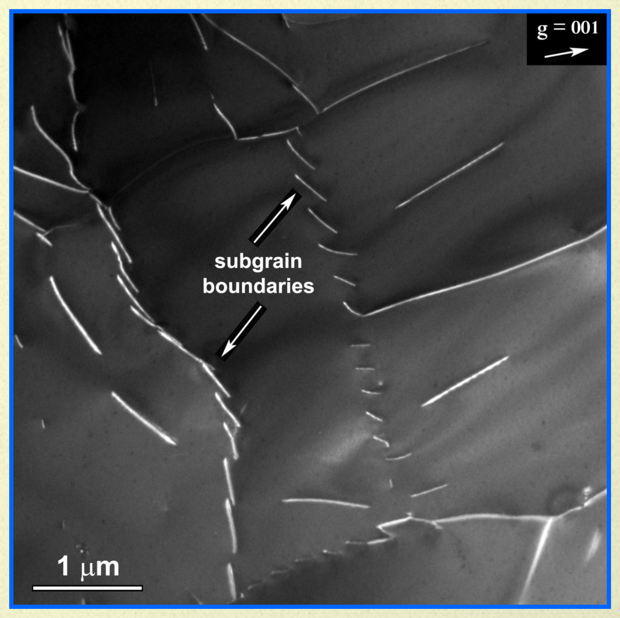

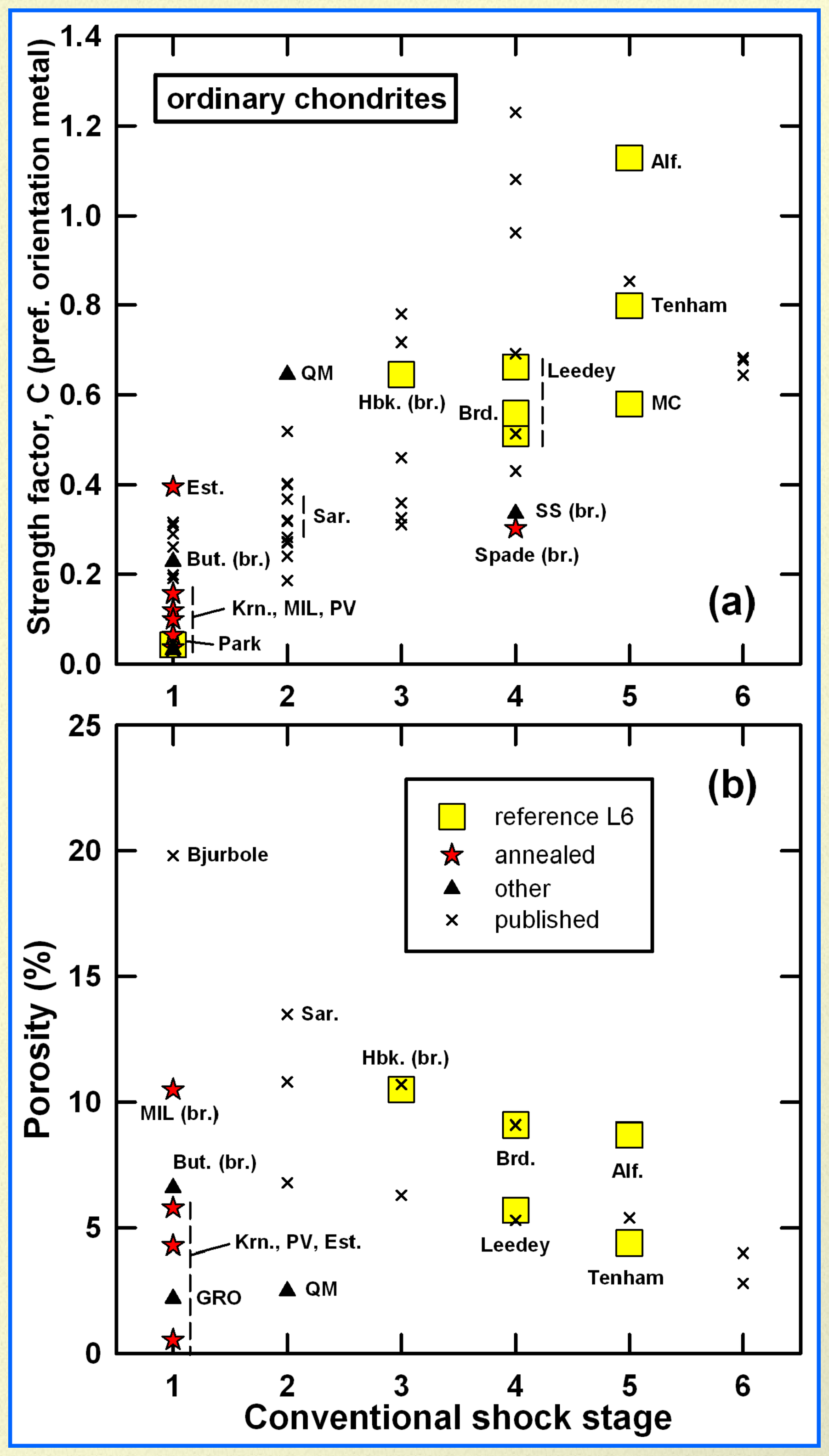

Fig. 4. Relationship between conventional shock stage and (a) strength factor C and (b) porosity. Abbreviations: br. = breccia; MIL = MIL 99301; PV = Portales Valley; Krn. = Kernouvé; Est. = Estacado; But. = Butsura; GRO = GRO 85209; QM = Queen's Mercy; Sar. = Saratov; Hbk. = Holbrook; Brd. = Bruderheim; SS = Saint-Séverin; Alf. = Alfianello; MC = Morrow County.

- Our data support the idea that metal grains were deformed and oriented by shock deformation [4, 5], as there is a rough correlation between shock stage and strength factor C (Fig. 4a)
- Given that metal grains become foliated, preferred orientation of metal arises by compaction of grains that behave in a ductile fashion during shock
- This implies porosity should reduce as compaction increases, supported for reference L chondrites and published meteorites by a crude inverse relationship between shock stage and porosity (Fig. 4b) and between strength factor C and porosity (Fig. 5)

Fig. 5. Relationship between strength factor C and porosity. Abbreviations as in Fig. 4.

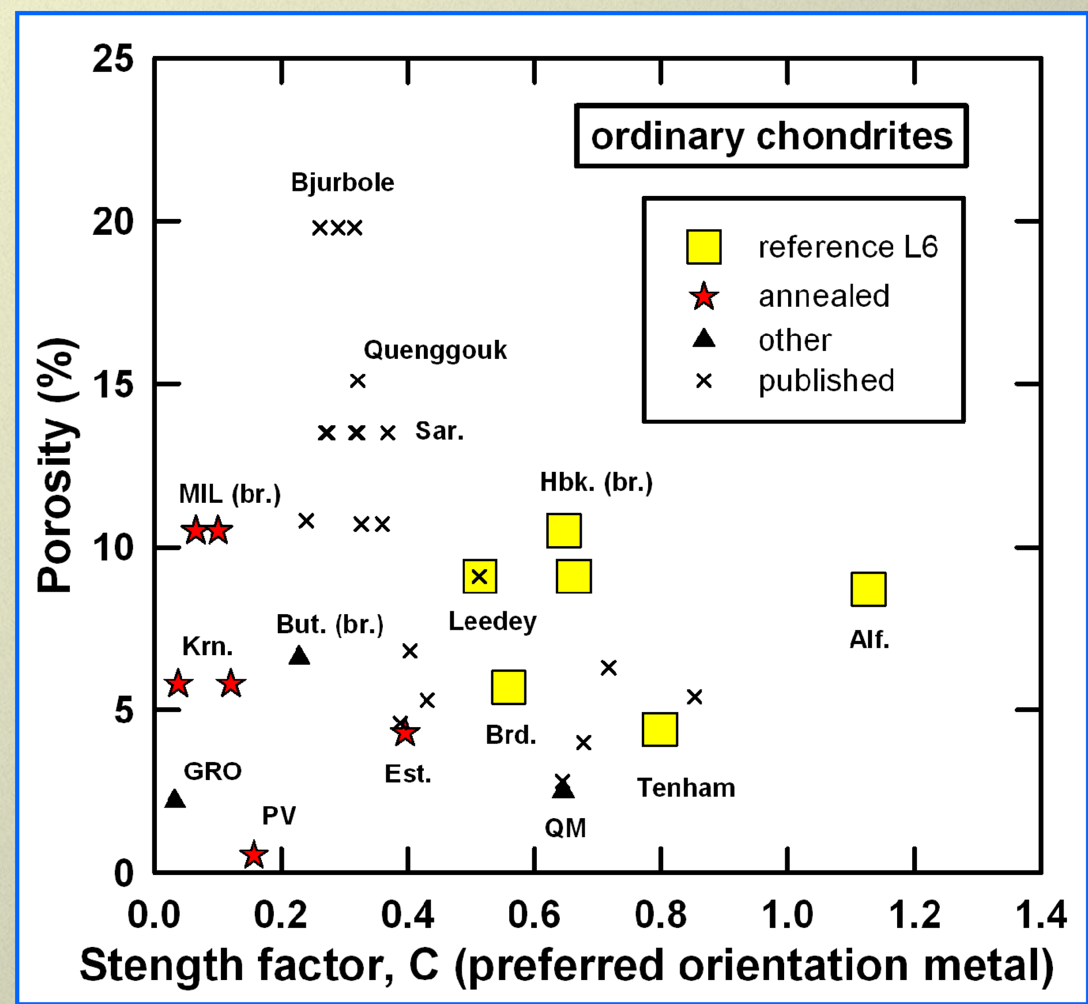

- "Annealed" low-shock meteorites have unexpectedly low porosities (Fig. 4b, 5)
- Microstructures suggest annealing and recovery obliterated strain and decreased shock stage [10, 15]; physical properties suggest elevated temperature during shock permitted additional compaction during deformation [2]

CONCLUSIONS

We conclude based on all available data that:

1) metal grains in ordinary chondrites behaved in a ductile fashion during shock deformation, allowing them to become progressively flattened with an increase in shock pressures;
2) there is support for the idea that shock deformation could have caused porosity reduction in some meteorites;
3) some apparently weakly-shocked chondrites with low metal grain flattening and low optical strain have anomalously low porosities, most of which show evidence for having been annealed, and some of which show evidence for having been deformed at elevated temperatures;
4) for annealed chondrites, elevated temperatures would have permitted additional compaction and porosity reduction during deformation, and annealing and microstructural recovery could have obliterated strain and caused a reduction in shock stage;
5) annealed chondrites probably formed at depth below an impact crater on an already warm body; heated planetesimals were impact-processed.

References: [1] Hirata et al. (1998) *LPS XXIX*, #1345. [2] Nakamura et al. (2001) *Icarus* 146, 289-300. [3] Hörz et al. (2005) *MAPS* 40, 1329-1346. [4] Friedrich et al. (2008) *EPSL* 275, 172-180. [5] Friedrich et al. (2014) *MAPS* 49, 1214-1231. [6] Hutson et al. (2007) *MAPS* 42, #5072. [7] Hutson et al. (2009) *LPS XXXX*, #1081. [8] Ruzicka & Hugo (2011) *MAPS* 74, #5368. [9] Ruzicka & Hugo (2014) XXXXV, #1306. [10] Ruzicka et al. (2015) In Press, *GCA*. [11] Ashworth & Barber (1977) *EPSL* 27, 43-50. [12] Friedrich et al. (2013) *GCA* 116, 71-83. [13] Scott et al. (2014) *GCA* 136, 13-37. [14] Rubin & Jones (2003) *MAPS* 38, 1507-1520. [15] Rubin (2004) *GCA* 68, 673-689. [16] Stöffler et al. (1991) *GCA* 55, 3845-3867. [17] Leroux et al. (1996) *MAPS* 31, 767-776.

Abstract 1544, 46th Lunar and Planetary Science Conference (2015).